Molecular Therapy
Original Article

Extracellular vesicles: Major actors of heterogeneity in tau spreading among human tauopathies

Elodie Leroux,[1,5] Romain Perbet,[1,5] Raphaëlle Caillierez,[1] Kevin Richetin,[2,3,4] Sarah Lieger,[1] Jeanne Espourteille,[2] Thomas Bouillet,[1] Séverine Bégard,[1] Clément Danis,[1] Anne Loyens,[1] Nicolas Toni,[2] Nicole Déglon,[3,4] Vincent Deramecourt,[1] Susanna Schraen-Maschke,[1] Luc Buée,[1] and Morvane Colin[1]

[1]Université de Lille, INSERM, CHU-Lille, Lille Neuroscience & Cognition, 59000 Lille, France; [2]Department of Psychiatry, Center for Psychiatric Neurosciences, Lausanne University Hospital (CHUV) and University of Lausanne, 1011 Lausanne, Switzerland; [3]Lausanne University Hospital (CHUV) and University of Lausanne, Neuroscience Research Center (CRN), Laboratory of Cellular and Molecular Neurotherapies, 1011 Lausanne, Switzerland; [4]Lausanne University Hospital (CHUV) and University of Lausanne, Department of Clinical Neuroscience (DNC), Laboratory of Cellular and Molecular Neurotherapies, 1011 Lausanne, Switzerland

Tauopathies are neurodegenerative diseases characterized by tau inclusions in brain cells. Seed-competent tau species have been suggested to spread from cell to cell in a stereotypical manner, indicating that this may involve a prion-like mechanism. Although the intercellular mechanisms of transfer are unclear, extracellular vesicles (EVs) could be potential shuttles. We assessed this in humans by preparing vesicles from fluids (brain-derived enriched EVs [BD-EVs]). These latter were isolated from different brain regions in various tauopathies, and their seeding potential was assessed *in vitro* and *in vivo*. We observed considerable heterogeneity among tauopathies and brain regions. The most striking evidence was coming mainly from Alzheimer's disease where the BD-EVs clearly contain pathological species that can induce tau lesions *in vivo*. The results support the hypothesis that BD-EVs participate in the prion-like propagation of tau pathology among tauopathies, and there may be implications for diagnostic and therapeutic strategies.

INTRODUCTION

Tau, a microtubule-associated protein,[1] aggregates into filaments in Alzheimer's disease (AD) and in other related and heterogeneous diseases called tauopathies, which are characterized by the intracellular accumulation of hyperphosphorylated tau.[2] An alternative splicing mechanism gives rise to six major isoforms of tau that coexist in the human brain, which either have three or four repeated sequences of the microtubule-binding region (3R-tau and 4R-tau).[3] In AD, tau protein principally aggregates into paired helical filaments (3R-tau and 4R-tau) within the neurons, while in progressive supranuclear palsy (PSP), tau aggregates consist of straight filaments (4R-tau) and are found in both the neurons and the glia. In Pick's disease (PiD), specific neuronal tau inclusions are seen, known as Pick bodies, in which 3R-tau aggregates to form a spherical shape within the neuronal cell body. These different tauopathy filaments are beginning to be better described and are different among tauopathies.[4–7]

In AD, the most common tauopathy, the progression of neurodegeneration in the brain correlates very well with the clinical signs of the disease at each stage. It follows a sequential, hierarchical progression of brain involvement in a pattern that is similar for all patients: the hippocampal formation, the polymodal association areas, the unimodal association regions, and in the final stages of the disease, the entire cerebral cortex.[8,9] This stereotypical hierarchy of neurodegeneration is known in the literature as the Braak stages.[8] Specific hierarchical pathways have also been described for PSP,[10,11] argyrophilic grain disease,[12] and PiD.[13] These patterns of progression have been considered as steps in the propagation of neurodegeneration and have led to the hypothesis of a prion-like tau propagation.[3] In this hypothesis, an abnormal tau protein conformation would lead to the prion-like transconformation of normal tau proteins into abnormal ones. This would be followed by the secretion of pathological seeds, which would then be internalized by healthy neurons, thus transmitting the pathology.

While tau was first identified as a protein implicated in the assembly and stabilization of microtubules,[1] it is now described as a pleiotropic protein with various cellular locations.[14] It is known that the protein can be secreted by unconventional pathways, mostly in a free form,[15–25] and it has also been found in extracellular vesicles (EVs).[26] EVs have two main cellular origins: (1) EVs known as exosomes are generated from multivesicular bodies, containing

Received 15 March 2021; accepted 20 September 2021;
https://doi.org/10.1016/j.ymthe.2021.09.020.

[5]These authors contributed equally

Correspondence: Morvane Colin, Université de Lille, INSERM, CHU-Lille, Lille Neuroscience & Cognition, Bâtiment Biserte, rue Polonovski, 59045 Lille Cedex, France.
E-mail: morvane.colin@inserm.fr
Correspondence: Luc Buée, PhD, Université de Lille, INSERM, CHU-Lille, Lille Neuroscience & Cognition, Bâtiment Biserte, rue Polonovski, 59045 Lille Cedex, France.
E-mail: luc.buee@inserm.fr

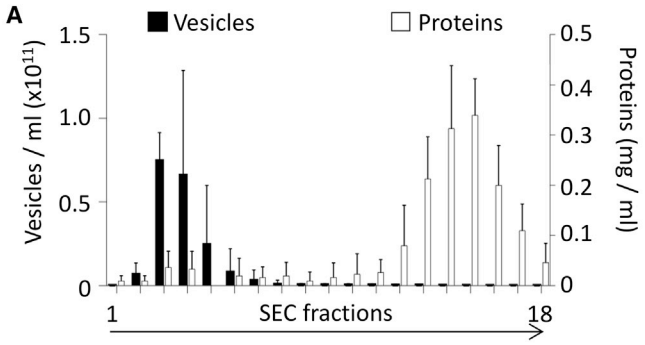

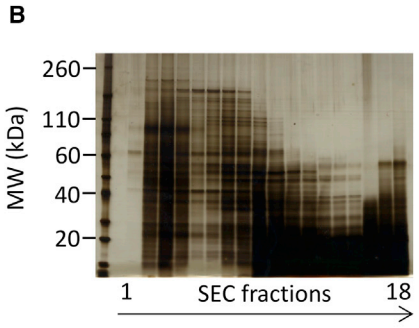

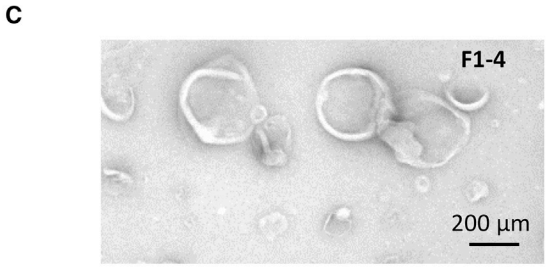

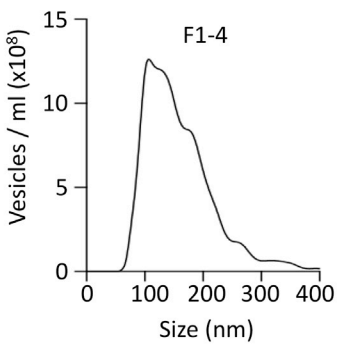

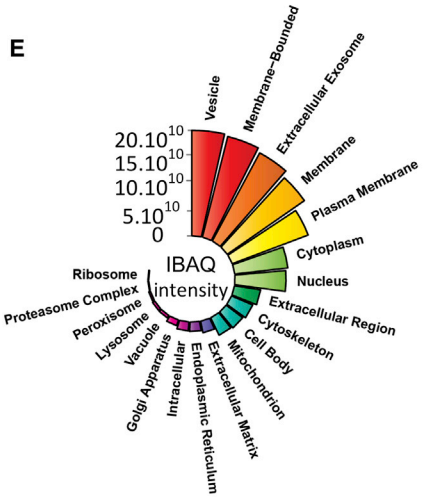

F

MISEV 2018 recommended category	1a	2a	3a	4a	5a
Detected	ADAM10; BSG; CD47; CD81; CD82; GNA*; HSPG*; IGTA*; IGTB*; LAMP1; LAMP2; NT5E; SDC*	ANXA*; ARF6; CHMP*; EHD*; FLOT1; FLOT2; HSP90AB1; HSPA8; MAPT; PDCD6IP; RHOA; SDCBP; TSG101; VPS4B	ALB; APOA1	HIST1H **	
Non-detected	CD55; CD59; CD63; H2-D; H2-D; H2-Q; HLA-A; HLA-B; HLA-C; SHH; TFR2	ARRDC1; CAV*; VPS4A	APOA2; APOB; APOB100	LMNA	EGF; FGF1; FGF2; TFNG; IL*; PDGF*; TGFB1; TGFB2; VEGFA

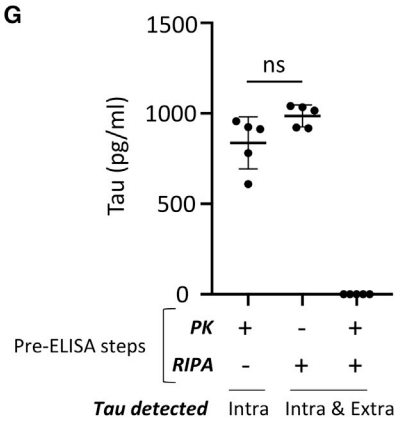

(legend on next page)

intraluminal vesicles, that are secreted into the extracellular fluid; and (2) EVs known as ectosomes originate from direct plasma membrane budding.[27] These vesicles have the capacity to transfer many biologically active molecules between cells, and they are known to be dysregulated in many disorders.[28] While the secretion of tau in EVs has been validated using many cell and animal models,[29] there are few data concerning the transfer of pathological tau species or seeds between cells[30] to induce a seeding process in humans.[31] According to the hypothesis of prion-like propagation, once inside the recipient cell, the seeds present in EVs seem to be released from the endolysosome and lead to the recruitment and misfolding of normal endogenous proteins.[32]

While tau aggregation is a common feature of tauopathies, a huge heterogeneity exists between and within these pathologies. Recent data suggest, for instance, that pathological tau seeds in human brains differ between tauopathies,[33] and also within a particular tauopathy, as has been shown for AD.[34] Additionally, the affected brain pathways differ between AD and other tauopathies, and some cell populations are more vulnerable than others.[8,11–13] It is thus essential to understand the underlying reasons for this heterogeneity before designing a specific therapeutic approach.

In this work, we focused our attention on EVs because they have a certain selectivity in terms of the target cell due to the presence of numerous ligands and receptors on their surface.[27] They therefore represent a unique intercellular delivery vehicle for transferring pathological species from one specific neuronal population to another, and they could explain the differing cell vulnerability seen in tauopathies. The work presented herein aims to compare the transmission of tau pathology via EVs that are present within brain-derived fluids (BD-fluids) of patients with various tauopathies. Although EVs isolated from the cerebrospinal fluid,[35–37] and plasma,[38–43] contain tau, the interstitial fluid (ISF) more accurately represents the environment around brain cells. This work therefore focuses on brain-derived enriched EVs (BD-EVs) in different tauopathies (AD, PSP, and certain forms of non-hereditary frontotemporal lobar degeneration with Pick bodies [formerly known as PiD]) as well as in non-demented controls. The seeding ability from BD-EVs purified from both tau transgenic mice and patients with various tauopathies is shown *in vitro*. In addition, AD BD-EVs are able to transmit tau pathology *in vivo* in a prion-like process. These results highlight the importance of defining how the pathology propagates through the brain in different tauopathies in order to design specific and tailored therapies as well as assessment tools for the evaluation of clinical trials.

RESULTS

In the present work, we isolated vesicles from the post-mortem BD-fluid of patients with various tauopathies, and we evaluated whether they contain species that are able to seed and spread the tau pathology in the brain.

EVs are present in the BD-fluid of a transgenic mouse model of tauopathy

To address this issue, we first isolated and characterized murine BD-EVs from a transgenic mouse model of tauopathy, the THY-tau30, that expresses human 1N4R tau protein with two pathogenic mutations (P301S and G272V) under the control of the neuron-specific Thy-1.2 promoter.[44,45] We prepared murine BD-fluids according to the protocol described by Polanco et al.[46] We then purified and characterized vesicles from the murine BD-fluid using size-exclusion chromatography (SEC). As it is critical to remove any aggregated or macroprotein contaminants associated with the BD-EVs, we purified them using SEC rather than classical ultracentrifugation procedures.[47] The concentration and distribution of the vesicles were analyzed by a nanoparticle tracking analysis (NTA) system, and the global protein content and its distribution were determined using UV detection or silver gel staining. SEC allowed us to efficiently enrich vesicles (fractions 1–4 [F1–4]) in our preparations from the protein contaminants, as previously described, while guaranteeing their morphological integrity (Figures 1A–1C). A size distribution of the BD-EV fractions revealed the presence of vesicles ranging from 50 to 400 nm (Figure 1D). Then, we used matrix-assisted laser desorption ionization-time of flight (MALDI-TOF) liquid chromatography-tandem mass spectrometry (LC-MS/MS) and quantitative analysis (intensity-based absolute quantification [IBAQ]) to evaluate F1–4 proteomic content. We identified a total of 2,064 proteins, of which 1,635 (79%) are referenced in the Vesiclepedia database. IBAQ scores combined with Gene Ontology cellular component (GOCC) annotation revealed that GOCC terms associated with EVs represent 76% of total IBAQ scores for the 20 selected terms (Figure 1E). Among proteins recommended by the Minimal Information for Studies of Extracellular Vesicles 2018 (MISEV2018),[48] we identified a majority of categories 1a (non-tissue-specific transmembrane or glycosylphosphatidylinositol [GPI]-anchored proteins), 2a (cytosolic proteins recovered in EVs), and 4a (transmembrane, lipid-bound, and soluble proteins associated to other intracellular compartments

Figure 1. Murine BD-EV characterization

Vesicles from murine BD-fluid were isolated using SEC to separate vesicles from free-floating proteins. They were separated by Sepharose resin columns in PBS and 500 μL per fraction was collected. (A and B) BD-EV concentration was quantified per fraction using NTA and expressed as vesicles/mL (A, filled columns); the amount of total protein was determined using either UV spectrophotometry (A, open columns) or a silver gel coloration (B). (C) Vesicle morphology was studied using electron microscopy in pooled fractions 1–4 (F1–4). The scale bar is indicated on the figure. (D) The size distribution of vesicles was determined using NTA in pooled F1–4. (E) Circular barplot showing IBAQ intensity scores obtained for 20 selected GOCC terms after quantitative proteomic analysis of F1–4. (F) Table listing human gene names corresponding to proteins recommended by MISEV2018 detected in F1–4 after MS-based proteomic analysis. An asterisk is used for families of multiple proteins; for example, for integrins, ITGA* indicates any integrin alpha chain. (G) The intravesicular tau (+PK−RIPA, with RIPA for ELISA tau detection) or the intra tau plus the extravesicular tau (−PK+RIPA) was quantified using ELISA from murine BD-EVs (3-month-old THY-tau30). A positive control showing the global lysis of tau is also shown (+PK+RIPA). ns, not significant. For (A) and (D), means of three independent experiments are shown; for (B) and (C), illustrative data are representative of at least three independent experiments.

than plasma membrane/endosomes) (Figure 1F). Among them are found the cytosolic vesicular markers HSP90 and tau protein (MAPT), which have been validated using either western blot (Figure S1A) or ELISA assays (Figure 1G). In addition, using a proteinase K (PK) digestion assay, we showed that tau is found inside BD-EVs and not associated to their outer leaflet. Indeed, the extravesicular proteolysis (PK^+, radioimmunoprecipitation assay buffer $[RIPA]^-$) does not affect intravesicular tau concentration, thus confirming tau as an intravesicular component (Figure 1G). This full characterization including NTA, silver gel staining, electron microscopy, proteomics, and western blot indicates that F1–4 contained vesicles and are enriched in EVs. This pool was considered as the BD-EVs fraction in the following experiments.

BD-EVs from a transgenic mouse model of tauopathy contain tau seeds

To determine the role of EVs in tau pathology spreading, the tau seeding content of BD-EVs prepared from 1-, 3-, and 6-month-old THY-tau30 mice (a transgenic mouse model with progressive tau lesions) was evaluated.[44,45] As controls, we also isolated BD-EVs from wild-type littermates and transgenic APP/PS1 mice (that develop amyloid deposition) that do not exhibit tau aggregation.[49] Tau lesions were examined in the brains of these animals using two well-characterized anti-tau antibodies (Abs): MC1[50] (tau conformational-dependent Ab) and AT100[51] (human phospho-dependent Ab that allowed the detection of insoluble/aggregated tau). MC1 (Figure S2a–g) and AT100 (Figure S2h–n) immunoreactivities were progressively detected in the hippocampal neurons of the CA1 layer of THY-tau30 mice from 1 to 6 months. Whereas few to no MC1 (Figure S2e) and AT-100 (Figure S2l) immunoreactivities were seen at 1 month of age, respectively, and MC1 immuno-positive neurites were easily detectable at 3 months with a few positive cell bodies (Figure S2f). A very slight AT100 immunostaining was also seen in 3-month-old mice in the subiculum (Figure S2m) when a strong immunoreactivity (in soma and neurites) was shown in 6-month-old animals by both MC1 and AT100 Abs (Figures S2g and n, respectively). No AT100 and MC1 immunoreactivities were observed in the wild-type littermates (Figures S2b–d and i–k) or in the transgenic APP/PS1 controls (Figures S2a and h). We then isolated vesicles of these murine BD-fluids and evaluated their ability to induce a nucleation process using a biosensor assay.[52] This involved a highly sensitive and quantitative assay using a novel fluorescence resonance energy transfer (FRET)-based biosensor cell line that specifically reports tau seeding activity. These cells express soluble forms of repeat domain (RD)-P301Stau-CFP and RD-P301Stau-yellow fluorescent protein (YFP). In the presence of seeds such as recombinant tau fibers, an oligomerization process allows energy transfer between CFP and YFP that is detectable by flow cytometry. BD-EVs were introduced inside the biosensor cells using Lipofectamine and the seeding activity was quantified. BD-EVs of THY-tau30 mice, unlike those obtained from the control lines (littermate of THY-tau30 and APP/PS1), contained seed-competent species (Figure 2A). In fact, the FRET signal was observed in an age-dependent manner only with THY-tau30 samples. The seeding effect was indeed related to BD-EVs since their removal by ultracentrifugation in F1–4 abolished the FRET signal (compare ultracentrifugation supernatant [no vesicle] to pellet [BD-EV fraction]) (Figure 2B). In addition, tau was mainly found within vesicles as demonstrated by tau immunodepletion after BD-EV sonication (Figure 2C). The sonication procedure was applied to ensure release of intravesicular tau and then facilitate its immunodepletion. Indeed, when intravesicular tau was immunodepleted, a 70% decrease in the FRET signal was observed (Figure 2D).

Taken together, these data strongly support the hypothesis that the progressive appearance of tau pathology in mice leads to the release of vesicles in the BD-fluid that contain seed-competent tau species.

The seeding capacity of BD-EVs is heterogeneous among human tauopathies

We showed that the presence of tau seeds inside BD-EVs is related to the progression of tau pathology in the case of mice. Given the heterogeneity among tauopathies, we questioned whether the seeding potential of BD-EVs would differ between these neurodegenerative diseases. Post-mortem brain samples of human non-demented controls (n = 5), AD (n = 10), PSP (n = 10), and PiD (n = 5) patients were obtained (Table 1) in order to isolate BD-EVs, as described above (Figure 1). Three brain regions (the prefrontal cortex, the occipital cortex, and the cerebellum) differentially affected by the pathology were dissected, and tau lesions were quantified by immunohistochemistry (IHC) using AT8, a phospho-dependent anti-tau Ab (Figures 3A and 3B). As expected, tau pathology is higher in AD cases. After SEC purification, the BD-EVs shared the same characteristics (size, morphology, content) as did those isolated from the murine brain (Figure S3). Additionally, the presence of a specific transmembrane tetraspanin associated with the vesicles was validated using immunogold electron microscopy (CD63; Figure S1B).

In contrast to the mice, where the whole brain was analyzed, only specific areas of the human brain were dissected for BD-fluid isolation. To avoid any bias, the results were systematically normalized according to the weight of the brain extracts used to prepare the BD-fluid. Our data showed that the vesicle concentrations (Figure 4A) and the global tau content (Figure 4B) did not differ among the tauopathies. Interestingly, BD-EVs from the brains of the controls contained global tau at a similar level than those from patients with tauopathies. This confirms that tau is physiologically secreted in EVs and gives new insight into the mode of tau secretion in human brain.

To determine whether the tau protein present in BD-EVs can induce a nucleation process and whether this is similar among tauopathies, BD-EVs were applied to biosensor cells, as before. The vesicular contents from the prefrontal and occipital regions of the AD BD-fluid induced a significant FRET signal compared to the non-demented controls. For BD-EVs from the PSP and PiD patients, a weak FRET signal was observed (Figure 4C), which was consistent with neuropathology (Figure 3). It is relevant to note that among the PiD samples, one had BD-EVs displaying a high FRET signal. This patient exhibited, in addition to Pick bodies, neurofibrillary tangles (NFTs) as seen in AD patients (Table 1), which could potentially account for this finding. Whereas

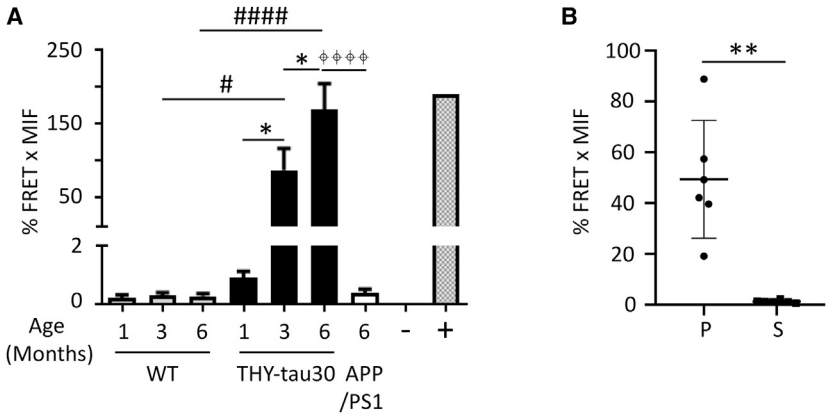

Figure 2. BD-EVs of a transgenic mouse model of tauopathy contain tau seeds

(A) BD-EVs of TgAPP/PS1 mice (6 months old, n = 6), wild-type littermate mice (1 [n = 8], 3 [n = 6], and 6 [n = 8] months old), and THY-tau30 mice (1 [n = 7], 3 [n = 8], and 6 [n = 8] months old) were applied to the HEK-tau biosensor cells, and the FRET signal was quantified using flow cytometry. 2 μM sonicated K18 fibrils were used as a positive control (+) and PBS was used as a negative control (−). (B) BD-EVs isolated from 3-month-old THY-tau30 mice (F1–4) were further ultracentrifuged to deplete vesicles. Pellet-containing vesicles (P) and supernatant (S) were applied to the biosensor assay. (C) Tau ELISA after tau immunodepletion (with or without sonication) from BD-EVs isolated from 3-month-old THY-tau30 mice. HT7 was used to immunodeplete tau, whereas IgG1 was used as a negative control of immunodepletion. (D) After tau immunodepletion of sonicated BD-EVs, fractions were applied to the biosensor assay. For (A), (B), and (D), results are expressed as the percentage of the FRET signal × MFI (% FRET × MFI). *$p < 0.05$, **$p < 0.01$; $^{\#}p < 0.05$, $^{\#\#\#\#}p < 0.0001$; $^{\Phi\Phi\Phi\Phi}p < 0.0001$.

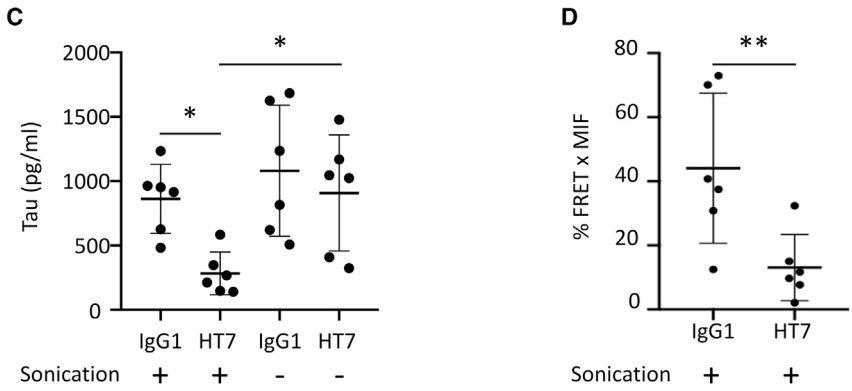

the FRET signal is related to the tau lesions in most cases (compare Figures 3B and 4C), as shown for the mice, the FRET signal for the AD cerebellum was significantly higher than that in the controls, even though both were devoid of tau lesions. This FRET signal did not reflect a passive release of intracellular vesicles due to cell death, as there was no correlation between the post-mortem delay and the FRET signal (Figure 4D). Taken together, our results demonstrate that although the global level of tau is similar in BD-EVs, the seeding/nucleation competency is clearly different according to the tauopathy considered, with a particularly high activity found in AD, in accordance with previous studies.[31]

BD-EVs are able to transmit tau pathology *in vivo*

To validate the seeding capacity of BD-EVs and to determine whether these vesicles are able to transmit tau pathology *in vivo*, we adapted our *in vivo* model of seeding.[53] This model is based on the intracerebral injection of material derived from AD brains into the hippocampi of 1-month-old THY-tau30 mice. At this age, the endogenous tau pathology is very weak,[44] thus allowing us to evaluate the seeding activity associated with the injected, human-derived material.

Four prefrontal cortex BD-fluid samples were pooled for each group: AD, PSP, PiD, and control. The BD-EVs were tested using the FRET assay (Figure 5A) before being injected into the animals (6×10^9 vesicles per hippocampus). A lower signal was generated for the PSP and PiD groups compared to the AD group, thus confirming what was previously shown *in vitro* (Figure 4C). These intact BD-EVs were then bilaterally injected in THY-tau30 mice and control littermates. Their respective ability to seed endogenous tau was monitored by IHC using MC1 (tau conformational-dependent Ab) or AT100 (human phospho-dependent Ab that allowed the detection of insoluble/aggregated tau) (Figure 5B). When the BD-EVs were injected into the wild-type mice, no MC1 or AT100 immunoreactivity was observed. No seeding occurred, and the tau species contained within the vesicles were not detected. In contrast, tau seeding was seen when BD-EVs from AD patients were injected in the THY-tau30 mice. MC1 and AT100 immunoreactivities were quantified. In contrast, injected BD-EVs from PSP and PiD did not induce any higher MC1 or AT100 immunoreactivity than did BD-EVs purified from human control brains (Figures 5C and 5D, respectively). This lower seeding capacity of BD-EVs from PSP and PiD than those from AD confirmed our *in vitro* data (Figure 4).

Altogether, our data show that BD-EVs containing tau seeds are capable of mediating the misfolding and phosphorylation of tau.

Table 1. Demographic, biological, and clinical characteristics of the human brain sample donors

Sex	Death (years)	PMD (h)	Diagnosis	Tau lesions	Braak	Thal stages	Cause of death
[a]M	78	19	Control	none	0	0	invasive aspergillosis
[a]F	82	NA	Control	none	1	1	pericarditis
[a]M	23	24	Control	none	0	0	myocarditis
[a]M	59	13	Control	none	0	0	Septic shock
M	41	11	Control	none	0	0	suffocation
M	70	30	AD	NFT	VI	4	
[b]F	63	15	AD	NFT	VI	4	
F	60	24	AD	NFT	VI	5	
F	82	84	AD	NFT	VI	5	
F	87	24	AD	NFT	VI	5	
[b]F	71	4	AD	NFT	VI	4	
M	64	20	AD	NFT	VI	4	
[b]M	66	27	AD	NFT	VI	5	
F	66	16	AD	NFT	VI	4	
[b]M	69	6	AD	NFT	VI	4	
[c]M	74	9	PSP	NFT and GFT	NA	1	
[c]M	90	36	PSP	NFT and GFT	NA	2	
M	88	3	PSP	NFT and GFT	NA	4	
[c]M	69	17	PSP	NFT and GFT	NA	0	
[c]F	79	4	PSP	NFT and GFT	NA	0	
M	65	18	PSP	NFT and GFT	NA	0	
M	82	4	PSP	NFT and GFT	NA	0	
M	64	18	PSP	NFT and GFT	NA	0	
F	77	9	PSP	NFT and GFT	NA	3	
M	57	20	PSP	NFT and GFT	NA	1	
[d]M	57	22	PiD	Pick bodies	NA	0	
[d]M	71	21	PiD	Pick bodies	NA	3	
[d]F	78	11	PiD	Pick bodies&NFT	NA	0	
[d]M	68	15	PiD	Pick bodies	NA	0	
M	68	8	PiD	Pick bodies	NA	0	

Demographic, biological, and clinical characteristics of the human brain sample donors- Brain samples used for BD-fluid isolation are listed (n = 5 non-demented controls, n = 10 AD, n = 10 PSP, and n = 5 PiD). PMD, post-mortem-delay.
[a]Non-demented controls.
[b]AD patients.
[c]PSP patients.
[d]PiD patients selected for the intracranial delivery of the BD-EVs in mice.

The data then strongly suggest the ability of the vesicular content to recruit and convert endogenous tau into an abnormal conformational form that differs among tauopathies, consistent with neuropathology, thus suggesting the existence of specific species inside the BD-EVs according to the particular tauopathy.

DISCUSSION

In this study, we investigated the role of BD-EVs in the heterogeneity and cell vulnerability of tauopathies. EVs possess ligands and/or receptors that are compatible with a specific cell type, and this could explain the neuronal selectivity and the hierarchy of neurodegeneration within tauopathies. To date, most studies have investigated the role of EVs in cell or animal models,[26,32,46,54,55] but few data are available for humans, especially when considering the ISF that is in direct contact with the brain cells and that is likely to be part of the prion-like process. The presence of EVs capable of transferring material between cells (Figures 5 and S4)[31,56] can help to explain the progression of the pathology in tauopathies. A very recent and elegant study carried out by Ruan et al.[31] showed for the first time that AD brain-derived EVs spread tau pathology with defined interneurons as their

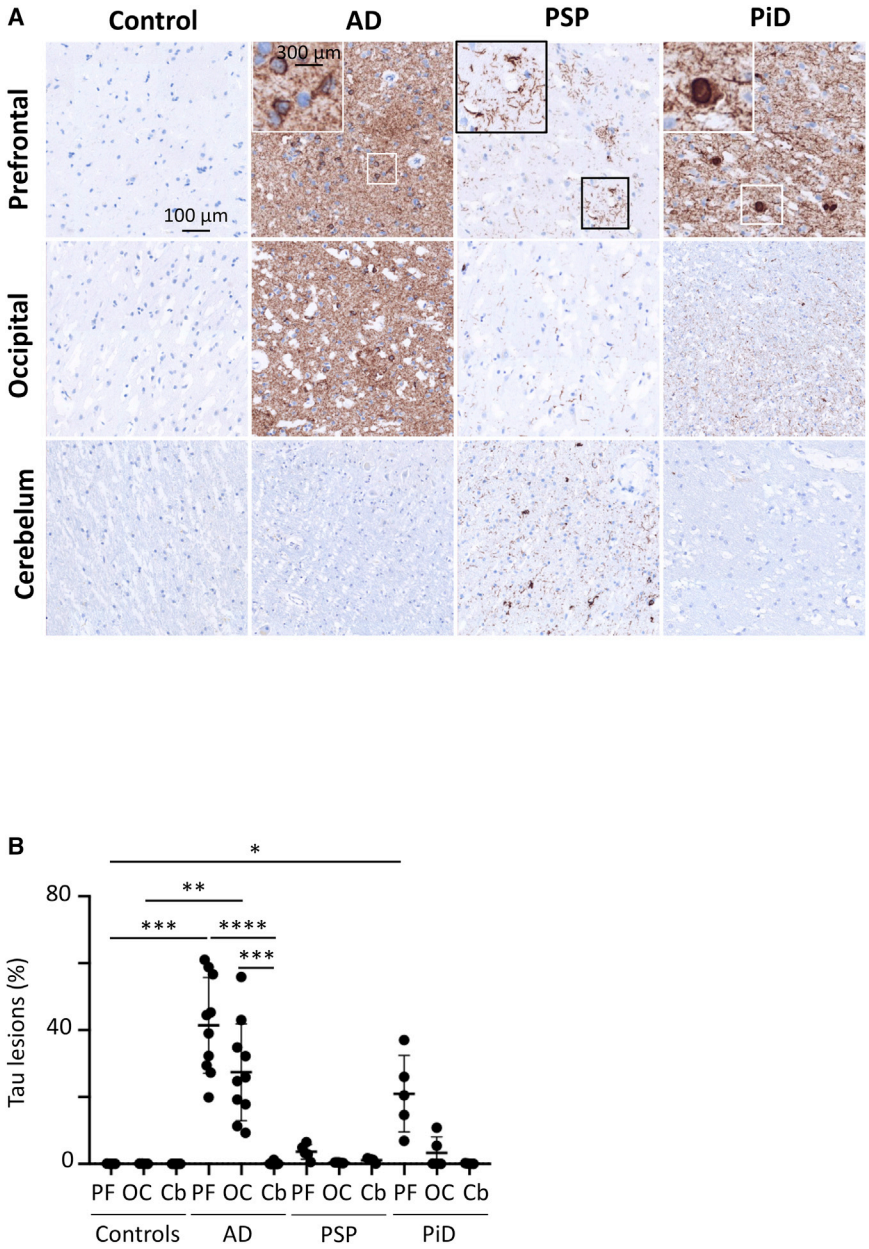

Figure 3. Tau lesions in human brain tauopathies

Prefrontal (PF), occipital (OC), and cerebellum (Cb) brain regions were dissected post-mortem from non-demented controls (n = 5) and patients with PSP (n = 5), PiD (n = 5), and AD (n = 10). (A) IHC of tau lesions using the AT8 antibody in mirror zones. Scale bars are indicated on the figure. (B) Human brain sections were blindly quantified using QuPath 0.2.1 software. Results are expressed as a percentage of tau lesions ([AT8-positive pixels/total pixels] × 100). *p < 0.05, **p < 0.01, ***p < 0.001, ****p < 0.0001.

target. Here, we go further into this mechanism by determining the contribution of vesicles to the heterogeneity of tauopathies by isolating and comparing BD-EVs from AD, PSP, and PiD, and from various brain regions differentially affected by the tau pathology.

Using our mouse models, we were able to (1) control the quality of BD-EV preparations, (2) demonstrate the role of BD-EVs-tau in the seeding process, and, most importantly, (3) highlight a link between BD-EV seeding capacity and the severity of the tau pathology. We confirmed these results in humans using brain regions that are differentially affected by the pathology (the prefrontal cortex, the occipital cortex, and the cerebellum), and the BD-EV seeding capacity was particularly striking in the case of AD. Specifically, BD-EVs from AD patients clearly contained seed-competent tau species (shown in the FRET assay), whereas such tau species were lower in the PSP and PiD materials. In general, tau pathology is much weaker in PSP and PiD than in AD, and this may contribute to the low seeding capacity of vesicles in these pathologies. However, other explanations are also possible: (1) although not unanimous, the prion-like propagation hypothesis may not be appropriate for PSP and PiD;[3] (2) a prion-like propagation may also exist for PSP and PiD, but EVs may not be the preferred shuttle, contrary to AD; and (3) the FRET assay used to measure seeding in PSP and PiD was less effective than in AD. In line with this latter possibility, previous studies found that PSP materials gave heterogeneous FRET signals.[33,57] Although a FRET signal was previously reported in PiD,[33] we did not observe a strong signal for most of the PiD cases in the present work. In fact, the only PiD patient showing a FRET signal also displayed NFTs, and this was the oldest PiD patient. We previously published that PiD patients displaying Pick bodies with additional NFTs have aging/AD-like materials, namely a pathological tau triplet revealed by immunoblotting.[58,59] The presence of such AD-like materials in this PiD patient could explain the high FRET signal as observed in the AD group.

Overall, our results suggest that the species shuttled by BD-EVs are very heterogeneous among tauopathies. What do we know about tauopathies? In PiD, there is an accumulation of 3R-tau in Pick bodies, and it is currently classified as frontotemporal lobar degeneration (FTLD)-tau.[60] Nevertheless, it is difficult to differentiate PiD and FTLD-tau with MAPT mutations (formerly FTDP-17). Both disorders have Pick bodies, but it has been shown that the Pick bodies are pS262-negative in PiD[61,62] and immunoreactive in FTLD-tau with

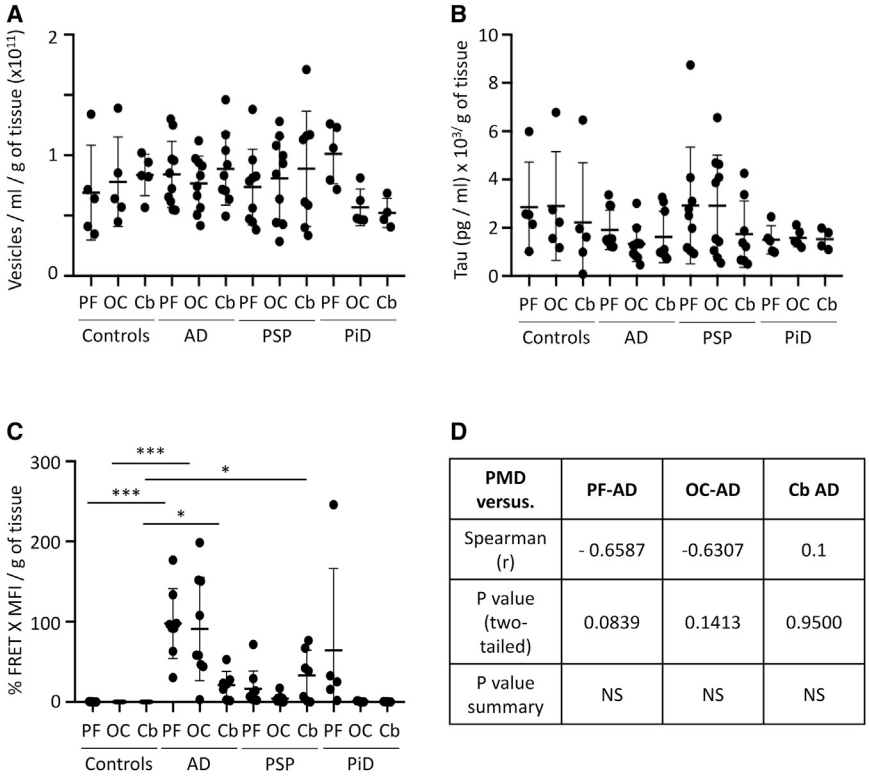

PMD versus.	PF-AD	OC-AD	Cb AD
Spearman (r)	- 0.6587	-0.6307	0.1
P value (two-tailed)	0.0839	0.1413	0.9500
P value summary	NS	NS	NS

Figure 4. Seed-competent species are found in BD-EVs in human tauopathies

BD-fluid was purified from the different brain regions and vesicles were isolated from 500 μL of BD-fluid. (A) BD-EV concentration was analyzed using NTA and expressed as vesicles/g/mL of tissue used to prepare the BD-fluid, and (B) global tau content was determined by ELISA (IN-NOTEST hTAU Ag, Fujirebio). Results are expressed as tau (pg/mL)/g of tissue. (C) BD-EVs were applied to the HEK-tau biosensor cells, and the FRET signal was quantified using flow cytometry. Results are expressed as % FRET × MFI/g of tissue. (D) Non-parametric Spearman correlation between the post-mortem delay (PMD) and the FRET signal generated by BD-EVs from the AD PF, AD OC, and AD Cb regions. *p < 0.05, ***p < 0.001.

MAPT mutations.[63,64] In any case, this lesion would appear to be particularly harmful because PiD often affects people who are relatively young (around 50 years of age), and it is characterized by very severe frontotemporal atrophy that is associated with neuronal death. Pick bodies are mostly found in layers II and VI of the frontotemporal isocortex and in the granular cell layer of the dentate gyrus.[59,65] These cells mainly express 3R-tau isoforms. It can therefore be postulated that these 3R-positive cells are fragile,[66] or else that the 3R-tau isoforms are more harmful than propagative.[67–69] In PSP, 4R-tau isoforms mostly aggregate to cause neurofibrillary degeneration. It is possible that the 4R-tau variants are secreted and captured by the glia. In line with this, both PSP and corticobasal degeneration are also characterized by gliofibrillary lesions.[60,70,71] Finally, in AD, all six tau isoforms aggregate, and neurofibrillary degeneration progresses in a hierarchical pathway from limbic, polymodal association, and unimodal association regions to the entire cerebral cortex. These observations suggest that tau seeds circulate in the ISF of AD brains. Our data support this hypothesis since tau seeds were identified in circulating EVs in all brain areas studied, even those devoid of tau lesions, such as the cerebellum. Depending on the brain area, EV receptor/ligand-bearing cells may or may not be present, which explains why some regions are affected by pathology while others are not. The combination of tau seeds in EVs and their ligand/receptor composition may therefore explain the neuronal selectivity/vulnerability and hierarchical pathway of neurodegeneration among tauopathies.

The molecular species involved in the pathological cycle of cell-to-cell transmission remain unknown, even though a great deal of work has been done to examine the roles of phosphorylation, truncation, oligomers, and high molecular weight species, among others.[29] Nevertheless, our work highlights the diversity of tau species inside BD-EVs among tauopathies, and it reinforces the hypothesis of prion-like propagation. It supports a transcellular transmission mechanism with a specificity that could explain the hierarchical and stereotypical propagation compatible with the Braak stages in AD.

Taken together, our data strongly support the existence of various tau species or co-factors inside BD-EVs among tauopathies, and their identification is now necessary in order to be able to determine the mechanism of tau pathology progression in these different diseases. The study raises a number of questions about therapeutic strategies, such as immunotherapy, that target free extracellular tau. Deciphering the nature of the pathological seeds found in the vesicles isolated from human brains, as well as the characteristics of the cargos/shuttles, will help in the design of specific tools aiming to block tau spreading.

MATERIALS AND METHODS

Abs

The following Abs were used for IHC, biochemical assays, and electron microscopy at the dilutions indicated below. The monoclonal Ab (mAb) AT8 recognizes the phosphoserine 202, phosphoserine 208, and phosphothreonine 205 residues of tau (MN1020; Thermo Scientific, Illkirch, France; 1:500 for IHC).[72] The mAb MC1 (a generous gift from Dr. Peter Davis; 1:1,000 for IHC) recognizes conformational changes, and its reactivity depends on both the N terminus (amino acids 7–9) and an amino acid sequence of tau (amino acids 313–322) in the third microtubule-binding domain.[50,73] The mAb AT100 (MN1060; Thermo Scientific, Illkirch, France; 1:500 for IHC)

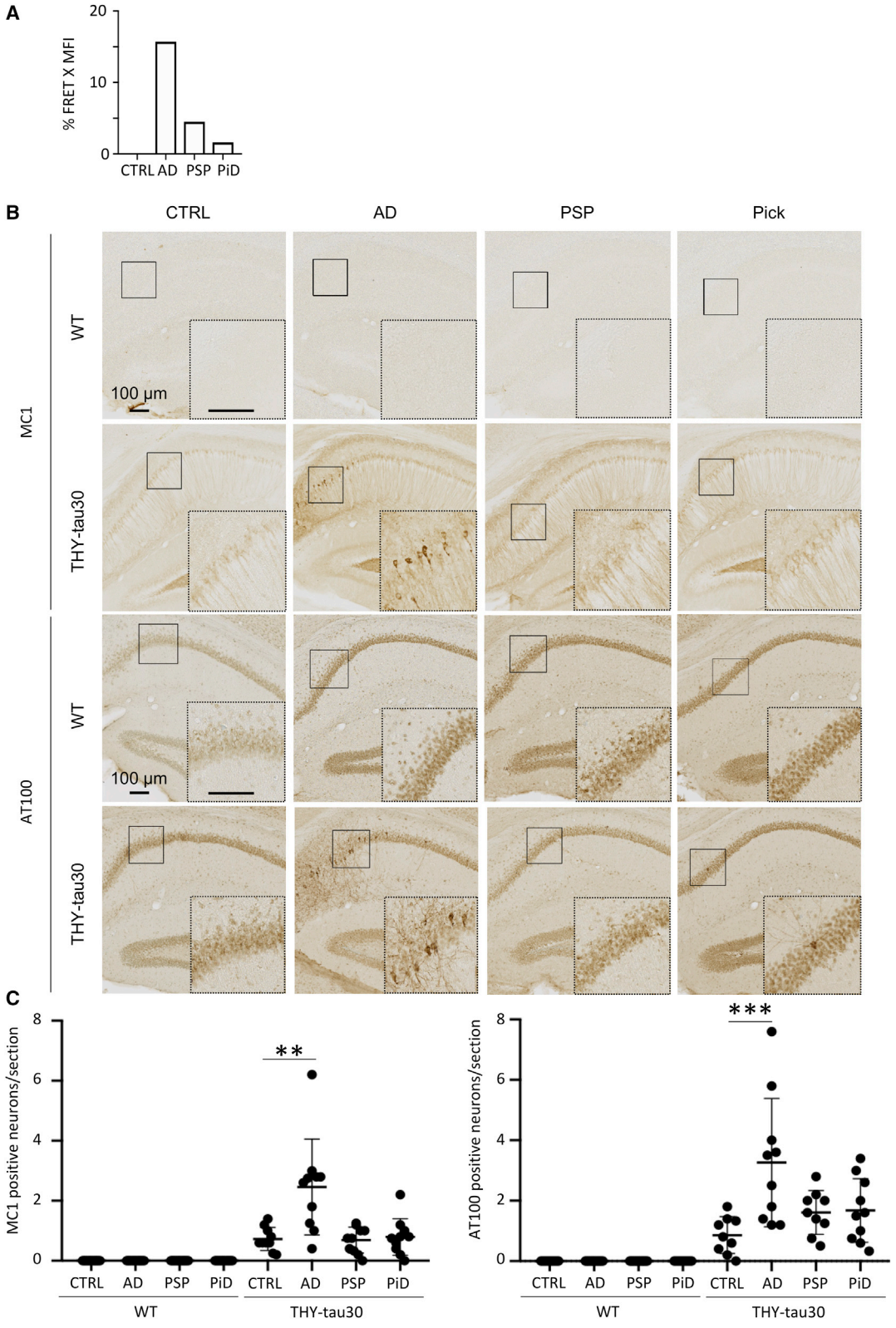

(legend on next page)

recognizes phosphothreonine 212 and phosphoserine 214 and allowed the detection of insoluble/aggregated tau.[51,74–76] The mAb HT7 (MN100; Thermo Scientific, Illkirch, France; used in the INNOTEST hTAU, as recommended by the manufacturer, Fujirebio) recognizes human tau (amino acids 159–163). Anti-heat shock protein (HSP) 90α/β (F-8; sc-13119; 1:100 for western blotting) is a mouse monoclonal antibody raised against amino acids 610-723 of HSP 90α/β of human origin. It is is recommended for detection of HSP 90α and HSP 90β of mouse, rat and human origin. Anti-CD63 is a mouse mAb (Novus Biologicals H5C6; nbp2-42225; 1:50 for electron microscopy), anti-NeuN is a rabbit mAb (Chemicon MAB377; 1:1000), and anti-V5 is a mouse mAb (Millipore AB3792; 1:500).

Animals and human samples

The study was performed in accordance with the ethical standards laid down in the 1964 Declaration of Helsinki and its later amendments. The experimental research was performed with the approval of an Ethics Committee (agreement APAFIS#2264-2015101320 441671 from CEEA75, Lille, France) and follows European guidelines for the use of animals. The animals (males and females) were housed in a temperature-controlled room (20°C–22°C) and maintained on a 12-h day/12-h night cycle with food and water provided *ad libitum* in a specific, pathogen-free animal facility (with five mice per cage or four rats per cage). Animals were randomly allocated to the different experimental groups. THY-tau30 mice were used that express human 1N4R tau protein with two pathogenic mutations (P301S and G272V) under the control of the neuron-specific Thy-1.2 promoter.[44,45]

Non-demented human control (n = 5), AD (n = 10), PSP (n = 10), and PiD (n = 5) brain extracts were obtained from the Lille Neurobank (fulfilling French legal requirements concerning biological resources and declared to the competent authority under the number DC-2008-642) with donor consent, data protection, and Ethics Committee approval. Samples were managed by the CRB/CIC1403 Biobank, BB-0033-00030. The demographic data are listed in Table 1.

Cell culture

The TauRDP301SFRET biosensor cells (ATCC CRL-3275), HEK293T cells, and HeLa cells were cultivated in Dulbecco's modified Eagle's medium with 10% fetal bovine serum, 1% GlutaMAX, and without HEPES. The cells were maintained in a humidified incubator with 5% CO_2. All cell lines were passaged twice a week. Rat primary cortical neurons were prepared from 17-day-old Wistar rat embryos, as previously described.[77] Ten days later, cells were infected with lentiviral vectors (LVs) encoding human 1N4R wild-type tau, as previously described.[78]

Brain-derived fluid isolation

BD-fluids were isolated as previously described.[46] For the frozen human brains, specific regions were removed (prefrontal cortex, occipital cortex, and cerebellum). 85 samples were used with a mean of 1.5 ± 0.07 g of tissue. Some brain areas were no longer available, that is, cerebellum (one AD, one PiD, and two PSP) and prefrontal cortex (one PSP). To avoid any bias in our results, normalization according to the weight of the brain extracts was systematically done.

For the mice, immediately after death, the whole brain (without the olfactory bulb and cerebellum) was recovered and frozen. The tissues were incubated on ice in 5 mL of Hibernate-A (50 mM NaF, 200 nM Na_3VO_4, 10 nM protease inhibitor [E64 from Sigma and protease inhibitor cocktail from Roche]). The tissues were gently mixed in a Potter homogenizer, and 2 mL of 20 U/mL papain (LS003119, Worthington Biochemical) in Hibernate-A was added to the homogenate for 20 min at 37°C with agitation. 15 mL of cold Hibernate-A buffer was then added and mixed by pipetting to stop the enzymatic activity. Successive centrifugations were applied at 4°C (300, 2,000, and 10,000 × *g*) to remove cells, membranes, and debris, respectively. The final supernatant was kept at −80°C before the BD-EV isolation procedures were applied.

BD-EV isolation

The procedures to isolate the BD-EVs from the murine or human BD-fluid were carried out in accordance with the MISEV guidelines that were established and updated in 2018 by the International Society for Extracellular Vesicles.[48] We applied various controls to validate the enrichment and the content of the BD-EVs, as recommended in these guidelines. However, the procedure described above to recover BD-fluids may lead to cell lysis. The presence of intraluminal vesicles in our preparations cannot be exclude. Because our fractions might be contaminated by ILVs, we refer them as BD-EVs. 500 μL of BD-fluid was loaded on the top of a SEC column (10-mL column, CL2B Sepharose, pore size 75 nm, Millipore).[79] This allowed us to recover a mean of 7.94×10^{10} ($\pm 3.36 \times 10^{9}$ vesicles/g of tissue in F1–4 (n = 85 samples). Isolation was carried out in phosphate-buffered saline (PBS) with a flow of 36–48 s/mL. The first 3 mL was eliminated and the following 20 fractions were recovered (with 500 μL per fraction). NTAs were performed on individual fractions diluted in PBS with a NanoSight NS300 (Malvern Panalytical). To generate statistical data, five videos of 90 s were recorded and analyzed using NTA software (camera level, 15; detection threshold, 4). When indicated, a further ultracentrifugation (100,000 × *g*, 50 min at 4°C, TLA110 rotor) was done.

Figure 5. AD BD-EVs efficiently seed host human mutated tau in young THY-tau30 mice

(A) Four AD, four PiD, four PSP, and four non-demented control BD-fluids were purified (Table 1), and isolated vesicles were pooled. 2 μL (6×10^9 vesicles) was applied to the HEK-tau biosensor cells, and the FRET signal was quantified using flow cytometry. Results are expressed as % FRET × MFI. (B) BD-EVs (6×10^9) were bilaterally injected into the hippocampi of 1-month-old THY-tau30 or wild-type mice littermates (n = 5). Mice were sacrificed 4 weeks post-injection and the tau pathology was analyzed by DAB immunostaining with the MC1 (upper) or AT100 (lower) antibodies. Sections from the hippocampus (injection site) are shown. Scale bars are indicated on the figure. (C) The numbers of MC1 (left) or AT100 (right) immunoreactive neurons per brain section were quantified (bregma −2.3 to −2.8 mm), and the data are presented as mean ± SD. $^{**}p < 0.01$, $^{***}p < 0.001$.

Electron microscopy

F1–4 from the SEC were pooled and concentrated to a final volume of 50 μL using Amicon Ultra 3K (Merck Millipore). Samples (5 μL) were deposited on a carbon film-supported grid (400 mesh) and incubated at room temperature (RT) for 20 min. For immunogold labeling, fixation in 2% paraformaldehyde (PFA; 0.1 M PO_4 buffer, pH 7.4) was performed for 20 min. Grids were rinsed for 2–3 min in PBS-glycine (50 mM) at RT. They were then soaked in a mixture containing 1% PBS-bovine serum albumin (BSA) and 1% normal goat serum for 1 h at RT before incubation with the primary Ab (1:50) in a mixture of 1% PBS-BSA and 1% normal goat serum, followed by rinsing in 0.1% PBS-BSA. Grids were then incubated for 1 h at RT with the appropriate goat anti-mouse secondary Ab (1:20, 12-nm colloidal gold) and finally washed in PBS. For immunogold labeling and morphological analyses, the grids were fixed in PBS-glutaraldehyde (1%) for 5 min at RT and then rinsed in distilled water. They were incubated for 5 min in 1% uranyl acetate and for 10 min on ice in a mixture containing 1% uranyl acetate/2% methylcellulose. Dry grids were observed under a transmission electron microscope (Zeiss EM900).

LC-MS/MS analysis

(1) Protein digestion: F1-4 fractions were digested according to a modified version of the iST method[80] (named miST method). Briefly, 50 μl solution in PBS were supplemented with in 50 μl miST lysis buffer (1% Sodium deoxycholate, 100 mM Tris pH 8.6, 10 mM DTT) and heated at 95°C for 5 min. Samples were then diluted 1:1 (v:v) with water and reduced disulfides were alkylated by adding $^1/_4$ vol of 160 mM chloroacetamide (final 32 mM) and incubating at 25°C for 45 min in the dark. Samples were adjusted to 3 mM EDTA and digested with 0.5 μg Trypsin/LysC mix (Promega #V5073) for 1h at 37°C, followed by a second 1h digestion with a second and identical aliquot of proteases. To remove sodium deoxycholate and desalt peptides, two sample volumes of isopropanol containing 1% TFA were added to the digests, and the samples were desalted on a strong cation exchange (SCX) plate (Oasis MCX; Waters Corp., Milford, MA) by centrifugation. After washing with isopropanol/1% TFA, peptides were eluted in 250 μl of 80% MeCN, 19% water, 1% (v/v) ammonia**; (2) Liquid chromatography-tandem mass spectrometry:** Eluates after SCX desalting were frozen, dried, and resuspended in variable volumes of 0.05% trifluoruacetic acid, 2% acetonitrile to equilibrate concentrations. Approximately 1 μg of each sample was injected on column for nanoLC-MS analysis; **(3) MS and MS data analysis:** dependent LC-MS/MS analysis of TMT sample was carried out on a Fusion Tribrid Orbitrap mass spectrometer (Thermo Fisher Scientific) interfaced through a nano-electrospray ion source to an Ultimate 3000 RSLCnano HPLC system (Dionex). Peptides were separated on a reversed-phase custom packed 40 cm C18 column (75 μm ID, 100Å, Reprosil Pur 1.9 μm particles, Dr. Maisch, Germany) with a 4-76% acetonitrile gradient in 0.1% formic acid (total time 140 min). Full MS survey scans were performed at 120'000 resolution. A data-dependent acquisition method controlled by Xcalibur 4.2 software (Thermo Fisher Scientific) was used that optimized the number of precursors selected ("top speed") of charge 2+ to 5+ while maintaining a fixed scan cycle of 1.5s. The precursor isolation window used was 0.7 Th. Full survey scans were performed at a 120'000 resolution, and a top speed precursor selection strategy was applied to maximize acquisition of peptide tandem MS spectra with a maximum cycle time of 0.6s. HCD fragmentation mode was used at a normalized collision energy of 32%, with a precursor isolation window of 1.6 m/z, and MS/MS spectra were acquired in the ion trap. Peptides selected for MS/MS were excluded from further fragmentation during 60s.

Tandem MS data were processed by the MaxQuant software (version 1.6.3.4)[81] incorporating the Andromeda search engine[82]. The UniProt reference proteome (RefProt) databases for Homo sapiens and mouse were used, supplemented with sequences of common contaminants. Trypsin (cleavage at K, R) was used as the enzyme definition, allowing 2 missed cleavages. Carbamidomethylation of cysteine was specified as a fixed modification. N-terminal acetylation of protein and oxidation of methionine were specified as variable modifications. All identifications were filtered at 1% FDR at both the peptide and protein levels with default MaxQuant parameters[83]. MaxQuant data were further processed with Perseus software[84], R statistical software and Microsoft Excel. We considered proteins as present in sample when unique + Razor Peptide Score >2 and an MS/MS Count >2. IBAQ values were calculated based on the summed intensities of all unique peptides for a protein divided by the number of theoretical tryptic peptides between 6 and 30 amino acids in length[85].

Western blotting and silver gel staining

Western blotting was performed as previously described.[86] Briefly, boiled samples (10 min, 100°C) were loaded onto a 4%–12% Bis-Tris NuPAGE Novex gel (Invitrogen), followed by transfer onto a 0.45-μm membrane using the Novex system from Life Technologies (XCell II blot module). The membrane was then incubated with blocking solution for 1 h at RT before incubation with the appropriate primary Ab overnight at 4°C. The membrane was then incubated for 1 h with the appropriate secondary Ab (horseradish peroxidase [HRP]-conjugated Ab, 1:50,000). The signal was visualized using enhanced chemiluminescence western blotting detection reagents (GE Healthcare). For silver gel staining, the same procedure was followed without the transfer onto a membrane. The gel was fixed overnight after migration in a mixture containing 40% ethanol and 10% acetic acid. Proteins were revealed by silver staining using the PlusOne silver staining kit and following the manufacturer's procedures (GE Healthcare).

Tau immunodepletion

BD-EV fractions were isolated from the BD-fluid of 3-month-old THY-tau30 mice. Immunodepletion of tau from F1–4 was performed using a Magna chromatin immunoprecipitation (ChIP) protein A+G magnetic beads (#16-663, Sigma-Aldrich). After 30 min in a water bath sonicator, F1–4 were incubated overnight with 2 μg of anti-tau Ab (HT7, #MN1000, Thermo Scientific) or control mouse monoclonal IgG1 Ab (GST [B-14]), Santa Cruz) with rotation at 4°C.

20 μL of magnetic beads was incubated with the complex Ab-antigen for 2 h with rotation at 4°C. A magnetic beads-Ab-antigen complex was isolated using a magnetic holder and the supernatant was collected.

PK treatment

A PK assay was done as previously described.[31,56] BD-EVs (lysis or not with radioimmunoprecipitation assay [RIPA] buffer) were incubated with 10 μg/mL PK for 30 min at 37°C to remove extravesicular proteins. The PK activity was then inhibited by adding 5 mM phenylmethylsulfonyl fluoride (PMSF) for 10 min at room temperature.

Recombinant K18 fibrils

The tau K18 recombinant protein and heparin were mixed to a ratio of 4:1 in aggregation buffer (HEPES at 10 mM, pH 6.9; NaCl at 1,000 mM) with a final protein concentration of 8 μM and incubated for 36–48 h at 37°C without shaking. The aggregation was confirmed at the end of the experiment by adding 50 μM thioflavin T to a 100 μL aliquot and comparing this to a negative control without the addition of heparin. The thioflavin T emission was detected at 490 nm after excitation at 440 nm using a PHERAstar (BMG Labtech, Ortenberg, Germany).

FRET assay

Cells were plated into a 12-well plate (150,000 cells per well) 24 h before treatment. Sonicated K18 fibrils (2 μM) were used as a positive control and PBS was the negative control. BD-EV fractions were pooled (F1–4) and concentrated in Amicon 3K columns to generate a final volume of 50 μL. The transfection mixture (50 μL of EVs + 50 μL of Opti-MEM plus 10 μL of Lipofectamine 2000 + 90 μL of Opti-MEM) was incubated for 20 min at RT and added to the cells. After 72 h, the cells were removed by scraping, and cell death was evaluated by adding Zombie NIR for 30 min at RT (as recommended by the manufacturer of the Zombie NIR fixable viability kit; BioLegend, 1:200). After one rinse in PBS, cells were fixed in 2% PFA for 10 min at RT and finally suspended in PBS for cytometry analyses using the flow cytometer Aria SORP (BD Biosciences; acquisition software FACSDiva v7.0, BD Biosciences) with the following excitation/emission wavelengths: excitation 405 nm, CFP emission 466 ± 40 nm and FRET YFP 529 ± 30 nm; excitation 488 nm, YFP emission 529 ± 30 nm. The FRET data were quantified using the Kaluza analysis software v2. Results are expressed as the percentage of FRET-positive cells × MFI (median fluorescence intensity). For the human brain samples, this value was normalized according to the weight of the tissue used to prepare the BD-fluid (percentage of FRET-positive cells × MFI/g of tissue).

Stereotaxic injections

Four BD-fluids (500 μL) were pooled for each of the AD, PSP, PiD, and control groups (Table 1), and the vesicles were isolated and concentrated to a final volume of 150 μL, as described above. For each of these, 2 μL (6×10^9 vesicles) was bilaterally injected into the hippocampi of 1-month-old anesthetized (100 mg/kg ketamine, 20 mg/kg xylazine) THY-tau30 mice and littermates (n = 5 per group; weight = 15–20 g), as done previously (anterior-posterior, −2.5 mm; medial-lateral, ±1 mm; dorsal-ventral, −1.8 mm to bregma).[53] The standard injection procedure involved the delivery of BD-EVs into THY-tau30 mice using a 10 μL Hamilton glass syringe with a fixed needle. After injection at a rate of 0.25 μL per minute, the needle was left in place for 5 min before removal to prevent any leakage of the injected material. For the experiments performed in rats (Figure S4), 3-month-old animals were anesthetized by intraperitoneal injection of a mixture of 100 mg/kg ketamine (Ketasol, Graeub, Bern, Switzerland) and 10 mg/kg xylazine (Rompun, Bayer Health Care, Uznach, Switzerland). The animals were bilaterally injected with 3 μL of BD-EVs into the dorsal dentate gyrus (anterior-posterior, −3 mm; medial-lateral, ±2.5 mm; dorsal-ventral, −3.4 mm to bregma). The vesicles were injected at a rate of 0.2 μL/min, and the needle was left in place for 5 min. In contrast to the FRET assay, in all *in vivo* experiments, intact BD-EVs were stereotactically injected without any Lipofectamine.

Tissue processing, IHC, and immunofluorescence

For the human brains, the different cerebral regions (the prefrontal cortex, the occipital cortex, and the cerebellum) were dissected, and the tau lesion quantification was performed using the mirror zones. For the mice, the whole brains were dissected and the tau lesions were quantified using dedicated mice. For the human brain sections, automated IHC was performed using 4-μm-thick formalin-fixed, paraffin-embedded (FFPE) tissue on a BenchMark Ultra (Roche Tissue Diagnostics) with the UltraView diaminobenzidine (DAB) IHC detection kit (Ventana) and the primary Ab AT8 (1:500). For the THY-tau30 and littermate mice, at 4 weeks post-injection they were deeply anesthetized and transcardially perfused with ice-cold 0.9% saline solution and subsequently with 4% PFA for 10 min. The brains were immediately removed, fixed overnight in 4% PFA, washed in PBS, placed in 20% sucrose for 24 h, and frozen until further use. Free-floating coronal sections (40 μm thick) were obtained using a cryostat microtome. For IHC, the brain sections were washed in PBS-0.2% Triton X-100, treated for 30 min at RT with 0.3% H_2O_2, and then washed three times. Non-specific binding was blocked using Mouse on Mouse reagent (1:100 in PBS, Vector Laboratories) for 60 min at RT. After three rinses in PBS-0.2% Triton X-100, the sections were incubated with the primary Ab MC1 (1:1,000) or AT100 (1:500) in PBS-0.2% Triton X-100 (1:1,000) overnight at 4°C. After three rinses in PBS-0.2% Triton X-100, labeling was amplified by incubation with anti-mouse biotinylated IgG (1:400 in PBS-0.2% Triton X-100, Vector Laboratories) for 60 min at RT. This was followed by a 120-min application of the avidin-biotin-HRP complex (ABC kit, 1:400 in PBS, Vector Laboratories) prior to the addition of diaminobenzidine tetrahydrochloride (Vector Laboratories) in Tris-HCl 0.2 mol/L (pH 7.6) containing 0.0015% H_2O_2 for visualization. Brain sections were then mounted, air-dried, dehydrated by passage through a graded series of alcohol (30%, 70%, 95%, 100%) and toluene baths, and finally mounted with VectaMount (Vector Laboratories). For the rats, 3 weeks after the BD-EV injections, they were deeply anesthetized and

transcardially perfused with 4% PFA. A series of one-in-six 30-μm-thick coronal sections were prepared and incubated at 4°C for 24 h in PBS containing 0.3% Triton X-100 with the following primary Abs: rabbit anti-NeuN and mouse anti-V5. After several rinses with PBS, the sections were incubated for 90 min at RT in a PBS solution containing a mixture of the appropriate secondary Abs: Alexa Fluor 488 and Alexa Fluor 555 mouse secondary Abs (1:500, Life Technologies). All of the sections were counterstained for 10 min with 4′,6-diamidino-2-phenylindole (DAPI; Merck; 1:5,000 dilution) to label the nuclei. IHC against V5/NeuN was followed by a final autofluorescence elimination step. To this end, autofluorescence eliminator reagent (EMD Millipore, 2160) was used, according to the manufacturer's instructions. Samples were mounted in Vectashield. Images were acquired (series of 50–75 multiple optical sections, z = 0.2 μm) with a Zeiss LSM 880 Quasar confocal system (×63 + ×4 numerical zoom) equipped with Airyscan.

Tau lesion quantification

For blinded quantification of MC1 and AT100 immunoreactivity, the CA1 region of the hippocampus was chosen as the quantification zone. We selected and quantified five brain sections covering the entire hippocampus (bregmas −2.30 to −2.8) and manually counted the number of MC1- or AT100-positive somas per brain section. Results are presented as the number of neurofibrillary tangles per brain section. Human brain sections were blindly quantified using QuPath 0.2.1 software for the full mirror image of the paraffin-embedded sections. Thresholds were established using a dedicated artificial intelligence algorithm (Artificial Neuronal Network; ANN_MLP) with identified objects on a set of slides, and these segmentation thresholds remained constant throughout the analyses. Results are expressed as a percentage of tau lesions ([AT8-positive pixels/total pixels] × 100).

Statistical analyses

Statistics and plots were generated using GraphPad Prism 8 software (version 8.0.0). The normality of the distributions was assessed graphically and using the Shapiro-Wilk test. In the case of a non-Gaussian distribution, the Mann-Whitney U test was used for one-to-one comparisons, and one-way non-parametric ANOVAs (Kruskal-Wallis) with a post hoc test were used for multiple comparisons. In the case of a Gaussian distribution, one-way ANOVAs with a post hoc test were used for multiple comparisons. Data are reported as the mean ± standard deviation (SD). Correlation analyses were performed using a non-parametric Spearman correlation test. The statistical tests adopted a two-tailed α level of 0.05.

SUPPLEMENTAL INFORMATION

Supplemental information can be found online at https://doi.org/10.1016/j.ymthe.2021.09.020.

ACKNOWLEDGMENTS

This work was supported by grants from the program Investissement d'Avenir LabEx (investing in the future laboratory excellence) DISTALZ (Development of Innovative Strategies for a Transdisciplinary Approach to Alzheimer's Disease), France Alzheimer, FONDATION ALZHEIMER (project EcTAUsome cohort), Fondation pour la Recherche Médicale, ANR grants (GRAND, TONIC), and by the PSP France Association. Our laboratories are also supported by LiCEND (Lille Centre of Excellence in Neurodegenerative Disorders), CNRS, Inserm, Métropole Européenne de Lille, University of Lille, I-SITE ULNE, Région Hauts de France, and FEDER. We are grateful to the Lille Neurobank and Prof. Claude-Alain Maurage for the access to the human brain samples. This study was also supported by a Synapsis Foundation fellowship awarded to K.R. and the Lausanne University Hospital (CHUV). The authors thank the Protein Analysis Facility of the University of Lausanne for technical support, in particular Dr. M. Quadroni. We also thank L. Culebras for help for circular graphical representation. We are grateful to the UMS-2014 US41 PLBS for access to the confocal microscopy and flow cytometry core facility platform at the HU site of the BioImaging Center Lille for help and for access to the cytometer. We thank Peter Davies for providing the MC1 antibody.

AUTHOR CONTRIBUTIONS

M.C. and L.B. designed and conceptualized the study, wrote the original draft, and then reviewed the manuscript. E.L, K.R., N.D., and N.T. helped with the manuscript editing; and E.L., R.P., R.C., S.L., T.B., S.B., V.D., A.L., S.S.-M., C.D., J.E., and K.R. performed the experiments.

DECLARATION OF INTERESTS

The authors declare no competing interests.

REFERENCES

1. Weingarten, M.D., Lockwood, A.H., Hwo, S.Y., and Kirschner, M.W. (1975). A protein factor essential for microtubule assembly. Proc. Natl. Acad. Sci. USA *72*, 1858–1862.

2. Spillantini, M.G., and Goedert, M. (2013). Tau pathology and neurodegeneration. Lancet Neurol. *12*, 609–622.

3. Colin, M., Dujardin, S., Schraen-Maschke, S., Meno-Tetang, G., Duyckaerts, C., Courade, J.P., and Buée, L. (2020). From the prion-like propagation hypothesis to therapeutic strategies of anti-tau immunotherapy. Acta Neuropathol. *139*, 3–25.

4. Falcon, B., Zhang, W., Schweighauser, M., Murzin, A.G., Vidal, R., Garringer, H.J., Ghetti, B., Scheres, S.H.W., and Goedert, M. (2018). Tau filaments from multiple cases of sporadic and inherited Alzheimer's disease adopt a common fold. Acta Neuropathol. *136*, 699–708.

5. Falcon, B., Zivanov, J., Zhang, W., Murzin, A.G., Garringer, H.J., Vidal, R., Crowther, R.A., Newell, K.L., Ghetti, B., Goedert, M., and Scheres, S.H.W. (2019). Novel tau filament fold in chronic traumatic encephalopathy encloses hydrophobic molecules. Nature *568*, 420–423.

6. Fitzpatrick, A.W.P., Falcon, B., He, S., Murzin, A.G., Murshudov, G., Garringer, H.J., Crowther, R.A., Ghetti, B., Goedert, M., and Scheres, S.H.W. (2017). Cryo-EM structures of tau filaments from Alzheimer's disease. Nature *547*, 185–190.

7. Duyckaerts, C., Bennecib, M., Grignon, Y., Uchihara, T., He, Y., Piette, F., and Hauw, J.J. (1997). Modeling the relation between neurofibrillary tangles and intellectual status. Neurobiol. Aging *18*, 267–273.

8. Braak, H., and Braak, E. (1991). Neuropathological stageing of Alzheimer-related changes. Acta Neuropathol. *82*, 239–259.

9. Delacourte, A., David, J.P., Sergeant, N., Buée, L., Wattez, A., Vermersch, P., Ghozali, F., Fallet-Bianco, C., Pasquier, F., Lebert, F., et al. (1999). The biochemical pathway of

neurofibrillary degeneration in aging and Alzheimer's disease. Neurology *52*, 1158–1165.

10. Verny, M., Duyckaerts, C., Agid, Y., and Hauw, J.J. (1996). The significance of cortical pathology in progressive supranuclear palsy. Clinico-pathological data in 10 cases. Brain *119*, 1123–1136.
11. Williams, D.R., Holton, J.L., Strand, C., Pittman, A., de Silva, R., Lees, A.J., and Revesz, T. (2007). Pathological tau burden and distribution distinguishes progressive supranuclear palsy-parkinsonism from Richardson's syndrome. Brain *130*, 1566–1576.
12. Saito, Y., Ruberu, N.N., Sawabe, M., Arai, T., Tanaka, N., Kakuta, Y., Yamanouchi, H., and Murayama, S. (2004). Staging of argyrophilic grains: An age-associated tauopathy. J. Neuropathol. Exp. Neurol. *63*, 911–918.
13. Irwin, D.J., Brettschneider, J., McMillan, C.T., Cooper, F., Olm, C., Arnold, S.E., Van Deerlin, V.M., Seeley, W.W., Miller, B.L., Lee, E.B., et al. (2016). Deep clinical and neuropathological phenotyping of Pick disease. Ann. Neurol. *79*, 272–287.
14. Sotiropoulos, I., Galas, M.C., Silva, J.M., Skoulakis, E., Wegmann, S., Maina, M.B., Blum, D., Sayas, C.L., Mandelkow, E.M., Mandelkow, E., et al. (2017). Atypical, non-standard functions of the microtubule associated Tau protein. Acta Neuropathol. Commun. *5*, 91.
15. Fontaine, S.N., Zheng, D., Sabbagh, J.J., Martin, M.D., Chaput, D., Darling, A., Trotter, J.H., Stothert, A.R., Nordhues, B.A., Lussier, A., et al. (2016). DnaJ/Hsc70 chaperone complexes control the extracellular release of neurodegenerative-associated proteins. EMBO J. *35*, 1537–1549.
16. Kang, S., Son, S.M., Baik, S.H., Yang, J., and Mook-Jung, I. (2019). Autophagy-mediated secretory pathway is responsible for both normal and pathological tau in neurons. J. Alzheimers Dis. *70*, 667–680.
17. Katsinelos, T., Zeitler, M., Dimou, E., Karakatsani, A., Müller, H.M., Nachman, E., Steringer, J.P., Ruiz de Almodovar, C., Nickel, W., and Jahn, T.R. (2018). Unconventional secretion mediates the trans-cellular spreading of tau. Cell Rep. *23*, 2039–2055.
18. Lee, J., and Ye, Y. (2018). The roles of endo-lysosomes in unconventional protein secretion. Cells *7*, 198.
19. Merezhko, M., Brunello, C.A., Yan, X., Vihinen, H., Jokitalo, E., Uronen, R.L., and Huttunen, H.J. (2018). Secretion of tau via an unconventional non-vesicular mechanism. cell rep. *25*, 2027–2035.e4.
20. Mohamed, N.V., Desjardins, A., and Leclerc, N. (2017). Tau secretion is correlated to an increase of Golgi dynamics. PLoS ONE *12*, e0178288.
21. Pooler, A.M., Phillips, E.C., Lau, D.H., Noble, W., and Hanger, D.P. (2013). Physiological release of endogenous tau is stimulated by neuronal activity. EMBO Rep. *14*, 389–394.
22. Rodriguez, L., Mohamed, N.V., Desjardins, A., Lippé, R., Fon, E.A., and Leclerc, N. (2017). Rab7A regulates tau secretion. J. Neurochem. *141*, 592–605.
23. Sato, C., Barthélemy, N.R., Mawuenyega, K.G., Patterson, B.W., Gordon, B.A., Jockel-Balsarotti, J., Sullivan, M., Crisp, M.J., Kasten, T., Kirmess, K.M., et al. (2018). Tau kinetics in neurons and the human central nervous system. Neuron *97*, 1284–1298.e7.
24. Sayas, C.L., Medina, M., Cuadros, R., Ollá, I., García, E., Pérez, M., Ferrer, I., Hernández, F., and Avila, J. (2019). Role of tau N-terminal motif in the secretion of human tau by End Binding proteins. PLoS ONE *14*, e0210864.
25. Tang, Z., Ioja, E., Bereczki, E., Hultenby, K., Li, C., Guan, Z., Winblad, B., and Pei, J.J. (2015). mTor mediates tau localization and secretion: Implication for Alzheimer's disease. Biochim. Biophys. Acta *1853*, 1646–1657.
26. Pérez, M., Avila, J., and Hernández, F. (2019). Propagation of tau via extracellular vesicles. Front. Neurosci. *13*, 698.
27. van Niel, G., D'Angelo, G., and Raposo, G. (2018). Shedding light on the cell biology of extracellular vesicles. Nat. Rev. Mol. Cell Biol. *19*, 213–228.
28. Maas, S.L.N., Breakefield, X.O., and Weaver, A.M. (2017). Extracellular vesicles: Unique intercellular delivery vehicles. Trends Cell Biol. *27*, 172–188.
29. Pernègre, C., Duquette, A., and Leclerc, N. (2019). Tau secretion: Good and bad for neurons. Front. Neurosci. *13*, 649.
30. Wang, Y.P., Biernat, J., Pickhardt, M., Mandelkow, E., and Mandelkow, E.M. (2007). Stepwise proteolysis liberates tau fragments that nucleate the Alzheimer-like aggregation of full-length tau in a neuronal cell model. Proc. Natl. Acad. Sci. USA *104*, 10252–10257.
31. Ruan, Z., Pathak, D., Venkatesan Kalavai, S., Yoshii-Kitahara, A., Muraoka, S., Bhatt, N., Takamatsu-Yukawa, K., Hu, J., Wang, Y., Hersh, S., et al. (2021). Alzheimer's disease brain-derived extracellular vesicles spread tau pathology in interneurons. Brain *144*, 288–309.
32. Polanco, J.C., Hand, G.R., Briner, A., Li, C., and Götz, J. (2021). Exosomes induce endolysosomal permeabilization as a gateway by which exosomal tau seeds escape into the cytosol. Acta Neuropathol. *141*, 235–256.
33. Sanders, D.W., Kaufman, S.K., DeVos, S.L., Sharma, A.M., Mirbaha, H., Li, A., Barker, S.J., Foley, A.C., Thorpe, J.R., Serpell, L.C., et al. (2014). Distinct tau prion strains propagate in cells and mice and define different tauopathies. Neuron *82*, 1271–1288.
34. Dujardin, S., Commins, C., Lathuiliere, A., Beerepoot, P., Fernandes, A.R., Kamath, T.V., De Los Santos, M.B., Klickstein, N., Corjuc, D.L., Corjuc, B.T., et al. (2020). Tau molecular diversity contributes to clinical heterogeneity in Alzheimer's disease. Nat. Med. *26*, 1256–1263.
35. Saman, S., Kim, W., Raya, M., Visnick, Y., Miro, S., Saman, S., Jackson, B., McKee, A.C., Alvarez, V.E., Lee, N.C., and Hall, G.F. (2012). Exosome-associated tau is secreted in tauopathy models and is selectively phosphorylated in cerebrospinal fluid in early Alzheimer disease. J. Biol. Chem. *287*, 3842–3849.
36. Spitzer, P., Mulzer, L.M., Oberstein, T.J., Munoz, L.E., Lewczuk, P., Kornhuber, J., Herrmann, M., and Maler, J.M. (2019). Microvesicles from cerebrospinal fluid of patients with Alzheimer's disease display reduced concentrations of tau and APP protein. Sci. Rep. *9*, 7089.
37. Muraoka, S., DeLeo, A.M., Sethi, M.K., Yukawa-Takamatsu, K., Yang, Z., Ko, J., Hogan, J.D., Ruan, Z., You, Y., Wang, Y., et al. (2020). Proteomic and biological profiling of extracellular vesicles from Alzheimer's disease human brain tissues. Alzheimers Dement. *16*, 896–907.
38. Fiandaca, M.S., Kapogiannis, D., Mapstone, M., Boxer, A., Eitan, E., Schwartz, J.B., Abner, E.L., Petersen, R.C., Federoff, H.J., Miller, B.L., and Goetzl, E.J. (2015). Identification of preclinical Alzheimer's disease by a profile of pathogenic proteins in neurally derived blood exosomes: A case-control study. Alzheimers Dement. *11*, 600–607.e1.
39. Guix, F.X., Corbett, G.T., Cha, D.J., Mustapic, M., Liu, W., Mengel, D., Chen, Z., Aikawa, E., Young-Pearse, T., Kapogiannis, D., et al. (2018). Detection of aggregation-competent tau in neuron-derived extracellular vesicles. Int. J. Mol. Sci. *19*, 663.
40. Jia, L., Qiu, Q., Zhang, H., Chu, L., Du, Y., Zhang, J., Zhou, C., Liang, F., Shi, S., Wang, S., et al. (2019). Concordance between the assessment of Aβ42, T-tau, and P-T181-tau in peripheral blood neuronal-derived exosomes and cerebrospinal fluid. Alzheimers Dement. *15*, 1071–1080.
41. Mustapic, M., Eitan, E., Werner, J.K., Jr., Berkowitz, S.T., Lazaropoulos, M.P., Tran, J., Goetzl, E.J., and Kapogiannis, D. (2017). Plasma extracellular vesicles enriched for neuronal origin: A potential window into brain pathologic processes. Front. Neurosci. *11*, 278.
42. Perrotte, M., Haddad, M., Le Page, A., Frost, E.H., Fulöp, T., and Ramassamy, C. (2020). Profile of pathogenic proteins in total circulating extracellular vesicles in mild cognitive impairment and during the progression of Alzheimer's disease. Neurobiol. Aging *86*, 102–111.
43. Winston, C.N., Goetzl, E.J., Akers, J.C., Carter, B.S., Rockenstein, E.M., Galasko, D., Masliah, E., and Rissman, R.A. (2016). Prediction of conversion from mild cognitive impairment to dementia with neuronally derived blood exosome protein profile. Alzheimers Dement. (Amst.) *3*, 63–72.
44. Leroy, K., Bretteville, A., Schindowski, K., Gilissen, E., Authelet, M., De Decker, R., Yilmaz, Z., Buée, L., and Brion, J.P. (2007). Early axonopathy preceding neurofibrillary tangles in mutant tau transgenic mice. Am. J. Pathol. *171*, 976–992.
45. Schindowski, K., Bretteville, A., Leroy, K., Bégard, S., Brion, J.P., Hamdane, M., and Buée, L. (2006). Alzheimer's disease-like tau neuropathology leads to memory deficits and loss of functional synapses in a novel mutated tau transgenic mouse without any motor deficits. Am. J. Pathol. *169*, 599–616.
46. Polanco, J.C., Scicluna, B.J., Hill, A.F., and Götz, J. (2016). Extracellular vesicles isolated from the brains of rTg4510 mice seed tau protein aggregation in a threshold-dependent manner. J. Biol. Chem. *291*, 12445–12466.

47. Böing, A.N., van der Pol, E., Grootemaat, A.E., Coumans, F.A., Sturk, A., and Nieuwland, R. (2014). Single-step isolation of extracellular vesicles by size-exclusion chromatography. J. Extracell. Vesicles *3*, 1.

48. Théry, C., Witwer, K.W., Aikawa, E., Alcaraz, M.J., Anderson, J.D., Andriantsitohaina, R., Antoniou, A., Arab, T., Archer, F., Atkin-Smith, G.K., et al. (2018). Minimal information for studies of extracellular vesicles 2018 (MISEV2018): A position statement of the International Society for Extracellular Vesicles and update of the MISEV2014 guidelines. J. Extracell. Vesicles *7*, 1535750.

49. Jankowsky, J.L., Slunt, H.H., Ratovitski, T., Jenkins, N.A., Copeland, N.G., and Borchelt, D.R. (2001). Co-expression of multiple transgenes in mouse CNS: A comparison of strategies. Biomol. Eng. *17*, 157–165.

50. Jeganathan, S., Hascher, A., Chinnathambi, S., Biernat, J., Mandelkow, E.M., and Mandelkow, E. (2008). Proline-directed pseudo-phosphorylation at AT8 and PHF1 epitopes induces a compaction of the paperclip folding of Tau and generates a pathological (MC-1) conformation. J. Biol. Chem. *283*, 32066–32076.

51. Allen, B., Ingram, E., Takao, M., Smith, M.J., Jakes, R., Virdee, K., Yoshida, H., Holzer, M., Craxton, M., Emson, P.C., et al. (2002). Abundant tau filaments and nonapoptotic neurodegeneration in transgenic mice expressing human P301S tau protein. J. Neurosci. *22*, 9340–9351.

52. Holmes, B.B., Furman, J.L., Mahan, T.E., Yamasaki, T.R., Mirbaha, H., Eades, W.C., Belaygorod, L., Cairns, N.J., Holtzman, D.M., and Diamond, M.I. (2014). Proteopathic tau seeding predicts tauopathy in vivo. Proc. Natl. Acad. Sci. USA *111*, E4376–E4385.

53. Albert, M., Mairet-Coello, G., Danis, C., Lieger, S., Caillierez, R., Carrier, S., Skrobala, E., Landrieu, I., Michel, A., Schmitt, M., et al. (2019). Prevention of tau seeding and propagation by immunotherapy with a central tau epitope antibody. Brain *142*, 1736–1750.

54. Polanco, J.C., Li, C., Durisic, N., Sullivan, R., and Götz, J. (2018). Exosomes taken up by neurons hijack the endosomal pathway to spread to interconnected neurons. Acta Neuropathol. Commun. *6*, 10.

55. Winston, C.N., Aulston, B., Rockenstein, E.M., Adame, A., Prikhodko, O., Dave, K.N., Mishra, P., Rissman, R.A., and Yuan, S.H. (2019). Neuronal exosome-derived human tau is toxic to recipient mouse neurons in vivo. J. Alzheimers Dis. *67*, 541–553.

56. Wang, Y., Balaji, V., Kaniyappan, S., Krüger, L., Irsen, S., Tepper, K., Chandupatla, R., Maetzler, W., Schneider, A., Mandelkow, E., and Mandelkow, E.M. (2017). The release and trans-synaptic transmission of Tau via exosomes. Mol. Neurodegener. *12*, 5.

57. Kaufman, S.K., Sanders, D.W., Thomas, T.L., Ruchinskas, A.J., Vaquer-Alicea, J., Sharma, A.M., Miller, T.M., and Diamond, M.I. (2016). Tau prion strains dictate patterns of cell pathology, progression rate, and regional vulnerability in vivo. Neuron *92*, 796–812.

58. Buée Scherrer, V., Hof, P.R., Buée, L., Leveugle, B., Vermersch, P., Perl, D.P., Olanow, C.W., and Delacourte, A. (1996). Hyperphosphorylated tau proteins differentiate corticobasal degeneration and Pick's disease. Acta Neuropathol. *91*, 351–359.

59. Hof, P.R., Bouras, C., Perl, D.P., and Morrison, J.H. (1994). Quantitative neuropathologic analysis of Pick's disease cases: Cortical distribution of Pick bodies and coexistence with Alzheimer's disease. Acta Neuropathol. *87*, 115–124.

60. Forrest, S.L., Kril, J.J., Stevens, C.H., Kwok, J.B., Hallupp, M., Kim, W.S., Huang, Y., McGinley, C.V., Werka, H., Kiernan, M.C., et al. (2018). Retiring the term FTDP-17 as *MAPT* mutations are genetic forms of sporadic frontotemporal tauopathies. Brain *141*, 521–534.

61. Delacourte, A., Sergeant, N., Wattez, A., Gauvreau, D., and Robitaille, Y. (1998). Vulnerable neuronal subsets in Alzheimer's and Pick's disease are distinguished by their tau isoform distribution and phosphorylation. Ann. Neurol. *43*, 193–204.

62. Mailliot, C., Sergeant, N., Bussière, T., Caillet-Boudin, M.L., Delacourte, A., and Buée, L. (1998). Phosphorylation of specific sets of tau isoforms reflects different neurofibrillary degeneration processes. FEBS Lett. *433*, 201–204.

63. Chaunu, M.P., Deramecourt, V., Buée-Scherrer, V., Le Ber, I., Brice, A., Ehrle, N., El Hachimi, K., Pluot, M., Maurage, C.A., Bakchine, S., and Buée, L. (2013). Juvenile frontotemporal dementia with parkinsonism associated with tau mutation G389R. J. Alzheimers Dis. *37*, 769–776.

64. Deramecourt, V., Lebert, F., Maurage, C.A., Fernandez-Gomez, F.J., Dujardin, S., Colin, M., Sergeant, N., Buée-Scherrer, V., Clot, F., Ber, I.L., et al. (2012). Clinical, neuropathological, and biochemical characterization of the novel tau mutation P332S. J. Alzheimers Dis. *31*, 741–749.

65. Buée, L., Bussière, T., Buée-Scherrer, V., Delacourte, A., and Hof, P.R. (2000). Tau protein isoforms, phosphorylation and role in neurodegenerative disorders. Brain Res. Brain Res. Rev. *33*, 95–130.

66. Richetin, K., Steullet, P., Pachoud, M., Perbet, R., Parietti, E., Maheswaran, M., Eddarkaoui, S., Bégard, S., Pythoud, C., Rey, M., et al. (2020). Tau accumulation in astrocytes of the dentate gyrus induces neuronal dysfunction and memory deficits in Alzheimer's disease. Nat. Neurosci. *23*, 1567–1579.

67. Dujardin, S., Bégard, S., Caillierez, R., Lachaud, C., Carrier, S., Lieger, S., Gonzalez, J.A., Deramecourt, V., Déglon, N., Maurage, C.A., et al. (2018). Different tau species lead to heterogeneous tau pathology propagation and misfolding. Acta Neuropathol. Commun. *6*, 132.

68. Sealey, M.A., Vourkou, E., Cowan, C.M., Bossing, T., Quraishe, S., Grammenoudi, S., Skoulakis, E.M.C., and Mudher, A. (2017). Distinct phenotypes of three-repeat and four-repeat human tau in a transgenic model of tauopathy. Neurobiol. Dis. *105*, 74–83.

69. Xu, C., Guo, J., Li, L., Wang, X., Zhou, Q., Sun, D., Zhang, S., Li, S., Ye, J., Liu, Y., et al. (2020). Co-expression of three wild-type 3R-tau isoforms induces memory deficit via oxidation-related DNA damage and cell death: A promising model for tauopathies. J. Alzheimers Dis. *73*, 1105–1123.

70. Rösler, M., Retz, W., Retz-Junginger, P., and Dennler, H.J. (1998). Effects of two-year treatment with the cholinesterase inhibitor rivastigmine on behavioural symptoms in Alzheimer's disease. Behav. Neurol. *11*, 211–216.

71. Jadhav, S., Avila, J., Schöll, M., Kovacs, G.G., Kövari, E., Skrabana, R., Evans, L.D., Kontsekova, E., Malawska, B., de Silva, R., et al. (2019). A walk through tau therapeutic strategies. Acta Neuropathol. Commun. *7*, 22.

72. Malia, T.J., Teplyakov, A., Ernst, R., Wu, S.J., Lacy, E.R., Liu, X., Vandermeeren, M., Mercken, M., Luo, J., Sweet, R.W., and Gilliland, G.L. (2016). Epitope mapping and structural basis for the recognition of phosphorylated tau by the anti-tau antibody AT8. Proteins *84*, 427–434.

73. Jicha, G.A., Bowser, R., Kazam, I.G., and Davies, P. (1997). Alz-50 and MC-1, a new monoclonal antibody raised to paired helical filaments, recognize conformational epitopes on recombinant tau. J. Neurosci. Res. *48*, 128–132.

74. Hoffmann, R., Lee, V.M., Leight, S., Varga, I., and Otvos, L., Jr. (1997). Unique Alzheimer's disease paired helical filament specific epitopes involve double phosphorylation at specific sites. Biochemistry *36*, 8114–8124.

75. Zheng-Fischhöfer, Q., Biernat, J., Mandelkow, E.M., Illenberger, S., Godemann, R., and Mandelkow, E. (1998). Sequential phosphorylation of Tau by glycogen synthase kinase-3beta and protein kinase A at Thr212 and Ser214 generates the Alzheimer-specific epitope of antibody AT100 and requires a paired-helical-filament-like conformation. Eur. J. Biochem. *252*, 542–552.

76. Yoshida, H., and Goedert, M. (2006). Sequential phosphorylation of tau protein by cAMP-dependent protein kinase and SAPK4/p38δ or JNK2 in the presence of heparin generates the AT100 epitope. J. Neurochem. *99*, 154–164.

77. Galas, M.C., Dourlen, P., Bégard, S., Ando, K., Blum, D., Hamdane, M., and Buée, L. (2006). The peptidylprolyl *cis/trans*-isomerase Pin1 modulates stress-induced dephosphorylation of Tau in neurons. Implication in a pathological mechanism related to Alzheimer disease. J. Biol. Chem. *281*, 19296–19304.

78. Dujardin, S., Bégard, S., Caillierez, R., Lachaud, C., Delattre, L., Carrier, S., Loyens, A., Galas, M.C., Bousset, L., Melki, R., et al. (2014). Ectosomes: A new mechanism for non-exosomal secretion of tau protein. PLoS ONE *9*, e100760.

79. Hagel, L., Östberg, M., and Andersson, T. (1996). Apparent pore size distributions of chromatography media. J. Chromatogr. A *743*, 33–42.

80. Kulak, N.A., Pichler, G., Paron, I., Nagaraj, N., and Mann, M. (2014). Minimal, encapsulated proteomic-sample processing applied to copy-number estimation in eukaryotic cells. Nat. Methods *11*, 319–324.

81. Cox, J., and Mann, M. (2008). MaxQuant enables high peptide identification rates, individualized p.p.b.-range mass accuracies and proteome-wide protein quantification. Nat. Biotechnol. *26*, 1367–1372.

82. Cox, J., Neuhauser, N., Michalski, A., Scheltema, R.A., Olsen, J.V., and Mann, M. (2011). Andromeda: A peptide search engine integrated into the MaxQuant environment. J. Proteome Res. *10*, 1794–1805.

83. Baietti, M.F., Zhang, Z., Mortier, E., Melchior, A., Degeest, G., Geeraerts, A., Ivarsson, Y., Depoortere, F., Coomans, C., Vermeiren, E., et al. (2012). Syndecan-syntenin-ALIX regulates the biogenesis of exosomes. Nat. Cell Biol. *14*, 677–685.

84. Tyanova, S., Temu, T., Sinitcyn, P., Carlson, A., Hein, M.Y., Geiger, T., Mann, M., and Cox, J. (2016). The Perseus computational platform for comprehensive analysis of (prote)omics data. Nat. Methods *13*, 731–740.

85. Schwanhäusser, B., Busse, D., Li, N., Dittmar, G., Schuchhardt, J., Wolf, J., Chen, W., and Selbach, M. (2011). Global quantification of mammalian gene expression control. Nature *473*, 337–342.

86. d'Orange, M., Aurégan, G., Cheramy, D., Gaudin-Guérif, M., Lieger, S., Guillermier, M., Stimmer, L., Joséphine, C., Hérard, A.S., Gaillard, M.C., et al. (2018). Potentiating tangle formation reduces acute toxicity of soluble tau species in the rat. Brain *141*, 535–549.